Bone Reports 12 (2020) 100242

Contents lists available at ScienceDirect

Bone Reports

journal homepage: www.elsevier.com/locate/bonr

Generation of an immunodeficient mouse model of tcirg1-deficient autosomal recessive osteopetrosis

Eleonora Palagano[a,b,1], Sharon Muggeo[a,b,1], Laura Crisafulli[a,b], Irina L. Tourkova[c], Dario Strina[a,b], Stefano Mantero[a,b], Elena Fontana[a,b], Silvia L. Locatelli[d], Marta Monari[e], Emanuela Morenghi[f], Carmelo Carlo-Stella[d,g], John B. Barnett[h], Harry C. Blair[c], Paolo Vezzoni[a,b], Anna Villa[a,b], Cristina Sobacchi[a,b,*,2], Francesca Ficara[a,b,2]

[a] CNR-IRGB, Milan Unit, via Fantoli 16/15, 20138 Milan, Italy
[b] Humanitas Clinical and Research Center IRCCS, via Manzoni 56, 20089 Rozzano, MI, Italy
[c] Veteran's Affairs Medical Center and Department of Pathology, University of Pittsburgh, 4200 Fifth Avenue, Pittsburgh, PA 15260, USA
[d] Department of Oncology and Hematology, Humanitas Clinical and Research Center IRCCS, via Manzoni 56, 20089 Rozzano, MI, Italy
[e] Clinical Investigation Laboratory, Humanitas Clinical and Research Center IRCCS, via Manzoni 56, 20089 Rozzano, MI, Italy
[f] Biostatistics Unit, Humanitas University, Rozzano, MI, Italy
[g] Department of Biomedical Sciences, Humanitas University, Rozzano, MI, Italy
[h] Department of Microbiology, Immunology, and Cell Biology, West Virginia University School of Medicine, Morgantown, WV 26505, USA

ARTICLE INFO

Keywords:
Osteopetrosis
Mouse model
Transplantation

ABSTRACT

Background: Autosomal recessive osteopetrosis is a rare skeletal disorder with increased bone density due to a failure in osteoclast bone resorption. In most cases, the defect is cell-autonomous, and > 50% of patients bear mutations in the *TCIRG1* gene, encoding for a subunit of the vacuolar proton pump essential for osteoclast resorptive activity. The only cure is hematopoietic stem cell transplantation, which corrects the bone pathology by allowing the formation of donor-derived functional osteoclasts. Therapeutic approaches using patient-derived cells corrected *ex vivo* through viral transduction or gene editing can be considered, but to date functional rescue cannot be demonstrated *in vivo* because a relevant animal model for xenotransplant is missing.
Methods: We generated a new mouse model, which we named NSG oc/oc, presenting severe autosomal recessive osteopetrosis owing to the *Tcirg1*^{oc} mutation, and profound immunodeficiency caused by the NSG background. We performed neonatal murine bone marrow transplantation and xenotransplantation with human CD34^{+} cells.
Results: We demonstrated that neonatal murine bone marrow transplantation rescued NSG oc/oc mice, in line with previous findings in the oc/oc parental strain and with evidence from clinical practice in humans. Importantly, we also demonstrated human cell chimerism in the bone marrow of NSG oc/oc mice transplanted with human CD34^{+} cells. The severity and rapid progression of the disease in the mouse model prevented amelioration of the bone pathology; nevertheless, we cannot completely exclude that minor early modifications of the bone tissue might have occurred.
Conclusion: Our work paves the way to generating an improved xenograft model for *in vivo* evaluation of functional rescue of patient-derived corrected cells. Further refinement of the newly generated mouse model will allow capitalizing on it for an optimized exploitation in the path to novel cell therapies.

1. Introduction

Osteopetrosis is a heterogeneous group of rare skeletal diseases, characterized by an increase in bone density due to defective bone resorption resulting from an alteration in osteoclast formation or function (Sobacchi et al., 2013). The autosomal recessive form (ARO) is the most severe, affecting children in early life and often leading to death if left untreated. The main clinical features of ARO are high bone density, reduced medullary space leading to pancytopenia, compression of cranial nerves, blindness and/or deafness; in addition, other multi-

* Corresponding author at: Humanitas Clinical and Research Center – IRCCS, via Manzoni 56, 20089 Rozzano, Italy.
E-mail address: cristina.sobacchi@humanitasresearch.it (C. Sobacchi).
[1] Co-first authorship.
[2] Co-last authorship.

https://doi.org/10.1016/j.bonr.2020.100242
Received 30 September 2019; Received in revised form 23 December 2019; Accepted 4 January 2020
Available online 07 January 2020

systemic defects (*e.g.* severe neurological defects) may be present (Sobacchi et al., 2013).

To date, hematopoietic stem cell transplantation (HSCT) is the only therapy (Penna et al., 2019). The outcome of this procedure is influenced by several factors: the age at the time of transplantation, the presence of secondary defects, the genetic defect and the availability of a compatible HLA donor. Regarding specifically this latter issue, in the absence of an HLA-matched donor, the probability of a successful transplant is variable and, despite substantial enhancement, HLA-haploidentical transplantation remains a procedure to be undertaken only in experienced centers (Bahr et al., 2016; Pronk et al., 2017; Neven et al., 2019; Stepensky et al., 2019). In recent years, an increasing number of ARO patients surviving until adulthood without a cure (hence classified as intermediate) have been reported (Sobacchi et al., 2014; Palagano et al., 2015; Sobacchi et al., 1993; Stattin et al., 2017). Despite a milder presentation as compared to "classical ARO", they accumulate debilitating skeletal (and extra-skeletal, as well) complications over time, thus prompting to consider the set-up of personalized therapeutic interventions (Stepensky et al., 2019; Neri et al., 2015; Teti and Econs, 2017). In particular, transplantation of *ex vivo* corrected autologous HSCs might represent a valid therapeutic option (Askmyr et al., 2009a). In 2007, the feasibility and efficacy of this approach was demonstrated in the oc/oc mouse model (Johansson et al., 2007), bearing a spontaneous homozygous genomic deletion in the *Tcirg1* gene (Frattini et al., 2005; Scimeca et al., 2000), which is also the most frequently mutated gene in ARO patients (Palagano et al., 2018). The *Tcirg1* gene encodes the a3 subunit of the osteoclast ATP-dependent vacuolar proton pump V-ATPase, essential for the acidification of the resorption lacuna and for osteoclast resorptive function (Frattini et al., 2000). Johansson and colleagues demonstrated that neonatal intraperitoneal infusion of oc/oc fetal liver cells transduced with a retroviral vector expressing TCIRG1 and GFP. This improved the survival of transplanted oc/oc mice, ameliorated their skeletal phenotype at 8 weeks and almost completely normalized it after 18 weeks (Johansson et al., 2007). Based on these encouraging results, lentiviral-mediated correction of the genetic defect in human cells was undertaken; their functional rescue was demonstrated *in vitro* after differentiation in bone-resorbing osteoclasts (Moscatelli et al., 2013; Thudium et al., 2016), while *in vivo* transplant in immunodeficient NSG mice proved their capacity to engraft (Moscatelli et al., 2018). Overall, these observations further fueled efforts towards the development of gene therapy for ARO. At the same time, the demonstration of *in vivo* functional rescue and amelioration of the disease by gene-corrected human cells could not be provided due to lack of a suitable animal model.

Immunodeficient animal models are largely used in human stem cell research as they can be engrafted with human cells thus allowing the assessment of human stem cell function *in vivo* (Manz and Di Santo, 2009; Fujiwara, 2018). In particular, the non-obese diabetic (NOD) SCID Il2r$\gamma^{-/-}$ (NSG) mice lack the adaptive immune response due to the defect in the *Prkdc* gene as well as the innate immune response (NK cells) due to the disruption of the *Il2r*γ gene (DiSanto et al., 1995), and express a *Sirpα* polymorphism that enhances the binding of mouse Sirpα to human CD47, thus preventing macrophage-mediated rejection of human cells (Takenaka et al., 2007).

We took advantage of this mouse model and, through an appropriate mating strategy, introduced the *Tcirg1*^{oc} mutation in the NSG background, eventually generating a new mouse model that we called NSG oc/oc, displaying osteopetrosis with immunodeficiency. Our findings set the bases for an improved xenograft model to evaluate *in vivo*, in a relevant murine condition, the efficacy of gene-corrected cells from ARO patients.

2. Methods

2.1. Animals

NOD.Cg-Prkdc^{scid} Il2rg^{tm1Wjl}/SzJ (NSG) (Shultz et al., 2005) and B6C3Fe a/a Tcirg1 oc/J-Ly5.2 (oc/+) mice were purchased from The Jackson Laboratory (Bar Harbor, ME); of note, prior to the present work, we had fully backcrossed the oc/+ mice on the C57BL/6J background.

Animals were group-housed in a specific-pathogen-free animal facility, under a 12-hour dark/light cycle, with water and food provided *ad libitum*. All the procedures involving mice were performed in accordance with ethical rules of the Institutional Animal Care and Use Committee of Humanitas Clinical and Research Center and with international laws (Italian Ministry of Health, protocol n.473/2017-PR).

2.2. Mouse genotyping

Mice were genotyped by PCR using DNA extracted from a tail biopsy. The PCR conditions for the *Prkdc* mutation were: 95 °C for 2 min, then 35 cycles, 95 °C for 30 s, 58 °C for 30 s and 72 °C for 1 min, then 72 °C for 5 min, with forward primer 5′-TTGAGCAGACAATGCT GAGAA-3′ and reverse primer 5′-TTCTGCATTCACAAGTCTTACCA-3′. The 157 base pair (bp) amplicon obtained was sequenced with the forward primer to identify the T-to-A transversion point mutation at position c.12138 in the *Prkdc* gene (ENSMUST00000023352.8).

For the *Il2r*γ gene, the targeted allele was identified by the presence of the Neomycin cassette, using the following PCR conditions: 95 °C for 2 min, then 35 cycles, 95 °C for 30 s, 55 °C for 30 s and 72 °C for 1 min, then 72 °C for 5 min, with forward primer 5′-GATGCTCTTCGTCCAGA TCA-3′ and reverse primer 5′-CTCCTGCCGAGAAAGTATCC-3′, producing a 150 bp amplicon in the presence of the Neo cassette; the wild type allele was detected through the same protocol using forward primer 5′-TCATGGGATGCATTGTCAGT-3′ and reverse primer 5′-CCTG GAGCTGGACAACAAAT-3′, producing a 234 bp amplicon (ENSMUST00000033664.13) in the absence of the Neo cassette.

For the *Tcirg1* gene, which in the oc/oc model carries a 1579 bp genomic deletion spanning from intron 1 to the 5′ of exon 3, genotyping was performed as previously described (Tondelli et al., 2009).

2.3. Tissue preparation and histology

Mice were sacrificed by CO_2 asphyxiation; tissues were harvested and either fixed in 4% paraformaldehyde (PFA) or processed to obtain cell suspensions for further analysis (see below). Selected bones were decalcified in an Ion Exchange Decal Unit (Biocare Medical, LLC, Pacheco, CA), dehydrated and embedded in paraffin for Hematoxylin and Eosin (H/E) staining. Other bones, after fixation, were decalcified in 14% ethylenediaminetetraacetic acid (EDTA), pH 7.4 with Acetic Acid, then dehydrated and embedded in paraffin for TRAP staining (Sigma-Aldrich, Saint Louis, MO). Von Kossa/Van Gieson staining was performed on plastic-embedded spine, according to standard procedures. Images were acquired with an Olympus BX51 Microscope (Olympus Optical Co., Ltd., Shinjuku, Tokyo, Japan).

For immunohistochemical staining, 3 μm thick longitudinal serial sections of formalin-fixed paraffin-embedded tissue were collected on glass slides, deparaffinized and treated for antigen retrieval, according to standard procedures. Tissue sections were incubated with 2% H_2O_2 for 15 min in the dark, washed with water and blocked with Rodent Block M (Biocare Medical) for 40 min at RT. Then, they were incubated overnight at 4 °C or 1 h at RT with the following primary antibodies: anti-mouse CD3 (SP7, 1:100; Thermo Fisher Scientific, Inc., Waltham, MA), anti-mouse B220 (1:300; eBioscience, Inc., San Diego, CA), anti-human CD45 (1:100; DAKO, Glostrup, Denmark), diluted in PBS 0.05% Tween 20 (PBST) (GIBCO®, Grand Island, NY, and Merck Millipore, Burlington, MA, respectively). Sections were then rinsed in PBST and

incubated with Mach 1 Polymer (Biocare Medical) for 30 min at RT, rinsed in PBST, developed with 3-3'-Diaminobenzidine (DAB) and counterstained with Hematoxylin. Images were acquired by an Olympus BX51 Microscope (Olympus Optical Co., Ltd).

2.4. Flow cytometry

Cell suspensions from spleens were prepared by meshing tissues in PBS with 2% fetal bovine serum (FBS) and 1 mM EDTA (FACS buffer) on a 40 μm filter followed by red blood cell lysis, and then incubated with the following monoclonal anti-mouse fluorescent-conjugated antibodies: TER-119 (TER-119), CD335 (29A1.4), CD11b (M1/70), CD8 (53-6.7), CD4 (RM4-5), B220 (RA3-6B2), IgM (II/41), IgD (Neri et al., 2015; Teti and Econs, 2017; Askmyr et al., 2009a; Johansson et al., 2007; Frattini et al., 2005; Scimeca et al., 2000; Palagano et al., 2018; Frattini et al., 2000; Moscatelli et al., 2013; Thudium et al., 2016; Moscatelli et al., 2018; Manz and Di Santo, 2009; Fujiwara, 2018; DiSanto et al., 1995; Takenaka et al., 2007; Shultz et al., 2005), F4/80 (BM8), Ly6C (AL-21), Ly6-G (1A8). Cell suspensions from thymuses were prepared by meshing tissues in FACS buffer on a 40 μm filter and then stained with the following monoclonal anti-mouse fluorescent-conjugated antibodies: CD45 (30-F11), CD8 (53-6.7), CD4 (RM4-5).

Bone marrow (BM) cell suspensions were prepared by crushing of multiple bones as described (Crisafulli et al., 2019); in general, we had already optimized this procedure to obtain enough cells for the analysis from osteopetrotic mice, in which BM encroachment and severe growth retardation dramatically reduce the total number of BM cells (Lo Iacono et al., 2012). Staining was performed as above, using monoclonal anti-human CD45 (2D1) and CD14 (61D3) fluorescent-conjugated antibodies. The same antibody cocktail was used for splenocytes obtained from transplanted mice.

For all described tissues, dead cell discrimination was performed with LIVE/DEAD™ Fixable Dead Cell Stain Kit (Thermo Fisher Scientific), following the manufacturer's instructions.

All samples were acquired on a BD FACSCanto II or an LSR Fortessa flow cytometer (BD Biosciences, Franklin Lakes, NJ) equipped with BD FACSDIVA™ software (BD Biosciences) and analyzed with FlowJo software v10.5.3 (FlowJo LLC, BD Biosciences). Antibodies were purchased from either BD Biosciences or eBioscience, Inc.

2.5. Serological analysis

Blood was collected at necropsy by cardiac puncture in the absence of anticoagulants, according to standard procedures. After few hours, serum was separated by low-speed centrifugation and samples were stored at −20 °C until use. Total calcium and phosphorus levels were determined using a Ci16200 Architect Abbott instrument (Abbott Park, IL, USA).

2.6. In vitro osteoclast differentiation and resorption assay

In vitro osteoclastogenesis was induced following standard protocols, as previously reported (Menale et al., 2019). Briefly, 4×10^5 splenocytes/well from NSG and NSG oc/oc littermates were cultured in 96-well plate in αMEM medium (Sigma-Aldrich) supplemented with 10% FBS, 1% penicillin/streptomycin (P/S) and 1% glutamine in the presence of 25 ng/ml murine Macrophage-Colony Stimulating Factor (M-CSF), 5 ng/ml human Transforming Growth Factor β1 (TGFβ1; both reagents from Peprotech, London, UK), 1 μM Dexamethasone (Sigma-Aldrich) and with or without 100 ng/ml murine Receptor Activator of Nf-kB Ligand (RANKL) for 6 days. Mature osteoclasts were stained using the Tartrate Resistant Acid Phosphatase (TRAP) Kit (Sigma-Aldrich) following the manufacturer's instruction.

The same culture conditions were applied to achieve osteoclast formation on dentin discs (Immunodiagnostic Systems, Ltd., Scottsdale, AZ) and evaluate their resorptive capacity. After 3 weeks, dentin discs were rinsed with water, scraped to remove attached cells, stained with 1% Toluidine blue solution for 3 min and then washed with water to visualize resorption pits. Images were acquired on an EVOS XL Inverted Microscope (Thermo Fisher Scientific) for both $TRAP^+$ mature osteoclasts and Toluidine blue-stained dentin discs.

2.7. Transplantation

For murine cell transplantation, 2–4 day old pups were irradiated with 100 centiGray (cGy) administered from a ^{137}Caesium (^{137}Cs) source. Four hours later, 10^7 total BM cells from 10 week old C57BL/6J donor mice were suspended in 30 μl PBS and injected into the temporal vein of recipient irradiated mice. After injection, the pups were returned to their cages. Mice were sacrificed by CO_2 inhalation at 2 timepoints: 3 weeks and 12 weeks post-transplantation.

For human cell transplantation, the radiation dose was 200 cGy, aiming at further favoring human cell engraftment. $1–2.6 \times 10^6$ $CD34^+$ cells from mobilized peripheral blood of consenting lymphoma patients (82–92% purity), were injected into NSG and NSG oc/oc recipient mice as above described. These $CD34^+$ cells are notoriously regarded as normal and in fact autologous hematopoietic stem cell transplantation is an established treatment for patients with hematologic malignancies (Castagna et al., 2015).

2.8. Micro-computed tomography (μCT)

MicroCT was performed using a Skyscan 1172 instrument (Bruker) at 6 μm resolution with 0.5 mm aluminum filter, source voltage 80 kV and current 100 uA. A 255 mg/ml cutoff was used for bone. Images were reconstructed using the NRecon and InstaRecon software (Bruker). Cross sectional images were obtained using Dataviewer software and three-dimensional images using the CTvox software (Bruker). Quantitative histomorphometric analysis of lumbar vertebrae and femoral bone were performed using the Bruker CTanalyser software.

2.9. Statistics

Statistical analysis was performed using Mann-Whitney test when comparing two groups. Kruskall-Wallis test was used for multiple comparisons (GraphPad Prism 6.0, GraphPad Softwares, Inc., La Jolla, CA). Statistical significance was considered when $p < 0.05$. All data are presented as mean ± SEM unless otherwise stated.

3. Results

3.1. Generation of the NSG oc/oc mouse model

In order to generate NSG oc/oc mice, first we bred NSG female mice with C57BL/6J oc/+ male mice. Fifty percent of the mice in the litters carried the mutations of the parental strains in the heterozygous state, on a NSG/C57BL/6J mixed background. These heterozygous mice were bred with NSG mice. In the generated litter, we selected individuals carrying the *Prkdc* and *Il2rγ* mutations in the homozygous state (hemizygous state for the *Il2rγ* mutation in male mice) and the *Tcirg1*^{oc} mutation in the heterozygous state (hereafter indicated as NSG oc/+ on a mixed background). These were crossed with NSG mice and the same breeding scheme was applied in the following four generations. Specifically, according to the Marker-Assisted Accelerated Backcrossing (MAX-BAX®) technology (Charles River Laboratories International, Inc., Wilmington, MA), which genotypes 384 carefully selected strain-specific single nucleotide polymorphisms, mice with allelic profiles most closely matching the profile of the recipient NSG strain, were mated to NSG mice to complete backcrossing for two additional generations. At the end, the NSG oc/+ colony was maintained in the heterozygous state due to early lethality of the NSG oc/oc mice, as further detailed below.

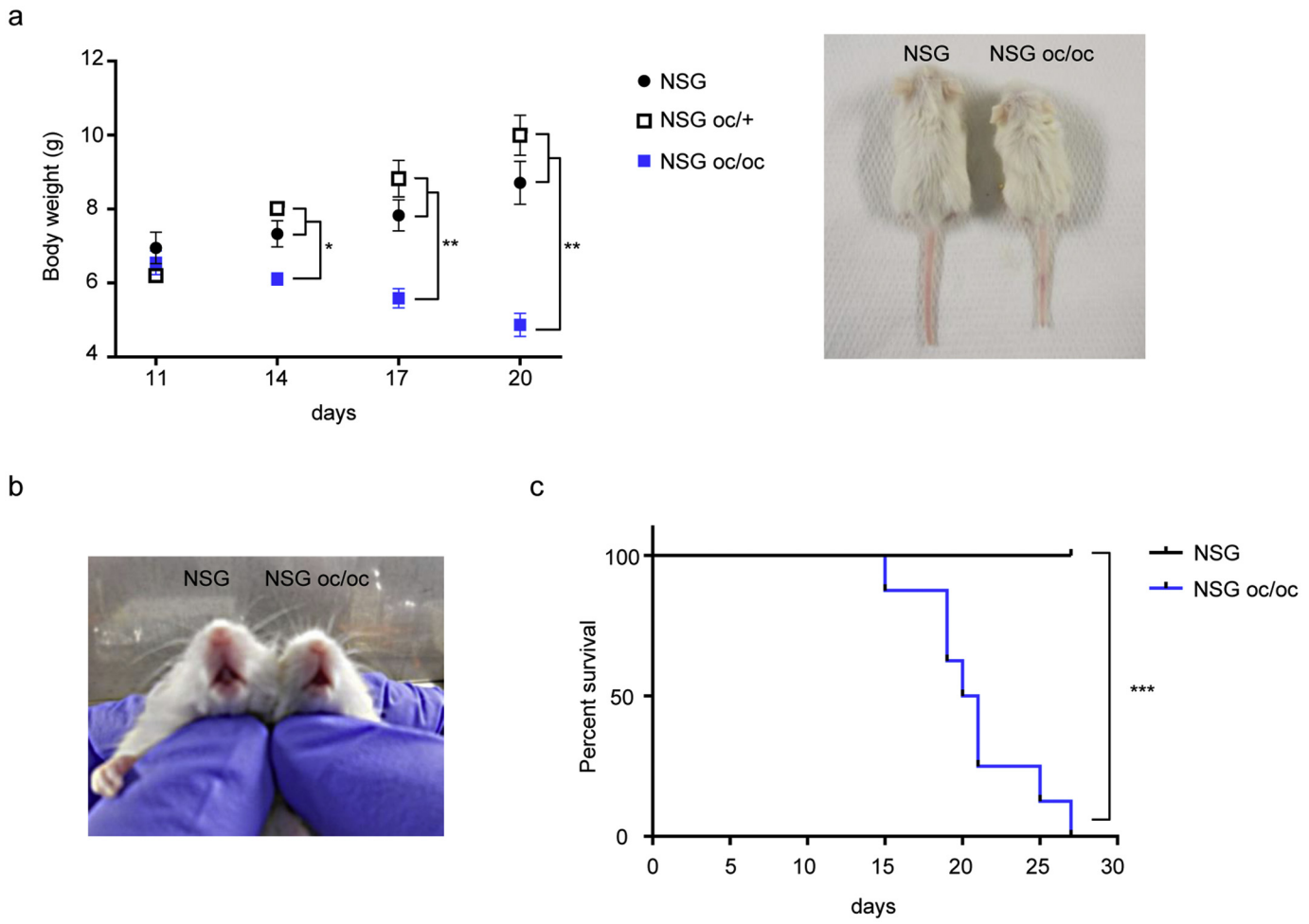

Fig. 1. The NSG oc/oc mouse model presents failure to thrive, lack of tooth eruption and reduced life span. a Left: body weight of NSG, NSG oc/+ and NSG oc/oc mice from post-natal day 11 (P11) to P20. NSG oc/+: $n \geq 3$; NSG and NSG oc/oc: $n \geq 6$. *$p < 0.05$; **$p < 0.01$. Right: representative photographs of NSG and NSG oc/oc littermates showing apparent reduced size in the latter. b Representative photographs of NSG and NSG oc/oc littermates showing lack of tooth eruption in the latter. c Kaplan-Mayer survival curves of NSG and NSG oc/oc mice (Log-rank test, ***$p < 0.0001$).

3.2. The NSG oc/oc mouse displays immunodeficiency and severe recessive osteopetrosis

Characteristic features of the parental strains used to generate the NSG oc/oc mouse are on one hand immunodeficiency with complete lack of B, T, and NK cells (Shultz et al., 2005), and on the other osteoclast rich-osteopetrosis with severe growth retardation, defective tooth eruption and extramedullary hematopoiesis (Frattini et al., 2005). Thus, we verified that the newly generated mouse model displayed these phenotypes.

NSG oc/oc mice were born at Mendelian ratio from NSG oc/+ breeding pairs; in total, litters comprised on average 8 pups each, as expected for the NSG strain in optimal housing conditions, and were regularly nursed, differently from what occurs with the parental oc/oc strain according to our experience. NSG oc/oc mice did not display an overt phenotype at birth, but around post-natal day 14 (P14) difference in body weight became apparent as compared to NSG and NSC oc/+ littermates (Fig. 1a), and tooth eruption failed to occur (Fig. 1b). In the following days, NSG oc/oc mice started displaying the so-called "circling behavior" typical of oc/oc mice, possibly due to worsening of the skull bone defect; moreover, they gradually lost weight, likely owing to poor nutrition. The severity of the disease importantly reduced their life span: in fact, 50% of NSG oc/oc mice died before weaning, and the remaining shortly after; none of them survived longer than 4 weeks (Fig. 1c). NSG oc/+ had a normal life span and were completely indistinguishable from NSG littermates, as expected based on the recessive nature of the *Tcirg1*^{oc} mutation; therefore, they were not further investigated.

To perform a deep characterization, we sacrificed NSG oc/oc and NSG littermates at P16-18; age matched C57BL/6J wild type (WT) mice were also included as positive controls for histology (Supplementary Fig. 1) and FACS analysis of the spleen (Supplementary Fig. 2a). At necropsy, the spleen was significantly enlarged in NSG oc/oc mice as compared to controls, and, considering the marked reduction of body weight in NSG oc/oc animals, the spleen weight/body weight ratio was even more strikingly increased (Fig. 2a). Tissue histology revealed that splenic architecture was completely disrupted in both NSG and NSG oc/oc mice: Hematoxilin/Eosin (H/E) staining showed absence of separation between red and white pulp and abundance of megakaryocytes, suggestive of intense extramedullary hematopoiesis, while immunohistochemical (IHC) staining with anti-CD3 and anti-B220 antibodies did not detect any T and B cells, respectively (Fig. 2b). Accordingly, total splenic cellularity was significantly higher in NSG oc/oc mice as compared to controls (Fig. 2c). Cytofluorimetric analysis of splenic cell suspensions showed that lymphocytes were virtually absent in NSG oc/oc and NSG littermates, with negligible numbers of T, B, and NK cells, as expected (Fig. 2c). The observed higher splenic cellularity in NSG oc/oc compared to NSG mice was accounted for by increased numbers of both myeloid and erythroid cells, with a 2- and 21-fold difference, respectively, resulting in a relative expansion of the

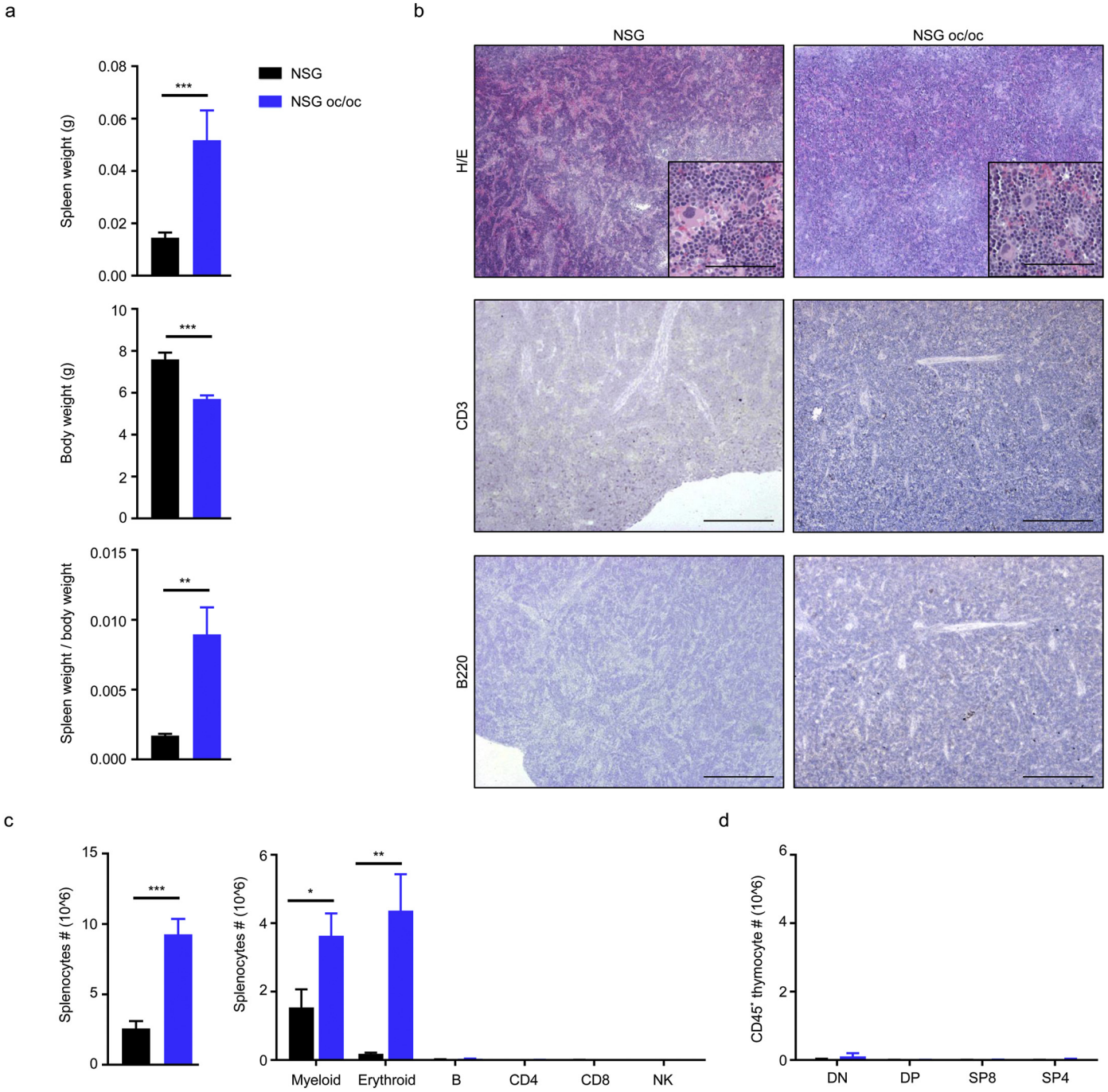

Fig. 2. The NSG oc/oc mouse model displays marked splenomegaly and severe immunodeficiency. a Spleen weight, body weight and spleen weight over body weight ratio in NSG and NSG oc/oc mice ($n \geq 7$ per genotype). b Representative images of formalin-fixed paraffin-embedded spleen sections from NSG and NSG oc/oc mice, stained with Hematoxylin/Eosin (H/E), anti-mouse CD3 or anti-mouse B220 antibody; positive controls are shown in Supplementary Fig. 1. Scale bar: 500 μm in the low magnification images, 100 μm in the inset. c Left: number of total splenocytes in NSG and NSG oc/oc mice ($n \geq 8$ per genotype). Right: number of cells of all main splenic cell subpopulations ($CD11b^+$ myeloid cells, $TER119^+$ erythroid cells, $B220^+$ B cells, $CD4^+$ and $CD8^+$ T lymphocytes, $NKp46^+$ NK cells) as determined by FACS analysis, following the gating strategy depicted in Supplementary Fig. 2 ($n \geq 5$ per genotype). d Number of double negative (DN), double positive (DP) and CD8, CD4 single-positive (SP8 and SP4) thymocytes after gating on $CD45^+$ hematopoietic cells, as described in Supplementary Fig. 3 ($n \geq 3$ per genotype). $^{**}p < 0.01$; $^{***}p < 0.001$.

erythroid compartment over the myeloid one, as likely expected during extramedullary hematopoiesis (Supplementary Fig. 2b). The thymus was almost undetectable in NSG oc/oc and NSG littermates, in accordance with the genetic defects in the *Prkdc* and *Il2rγ* genes. Moreover, in both groups FACS analysis showed only few residual double-negative thymocytes, with almost complete absence of immature double-positive and mature single-positive T cells (Fig. 2d and Supplementary Fig. 3).

Serological analysis revealed significantly reduced calcium and phosphate levels in NSG oc/oc mice as compared to controls (Fig. 3a). Derangements in calcium homeostasis point to altered bone metabolism. Indeed, H/E staining of decalcified paraffin-embedded bone sections showed very dense tissue containing cartilage remnants, loss of corticomedullary differentiation and extremely limited marrow space in

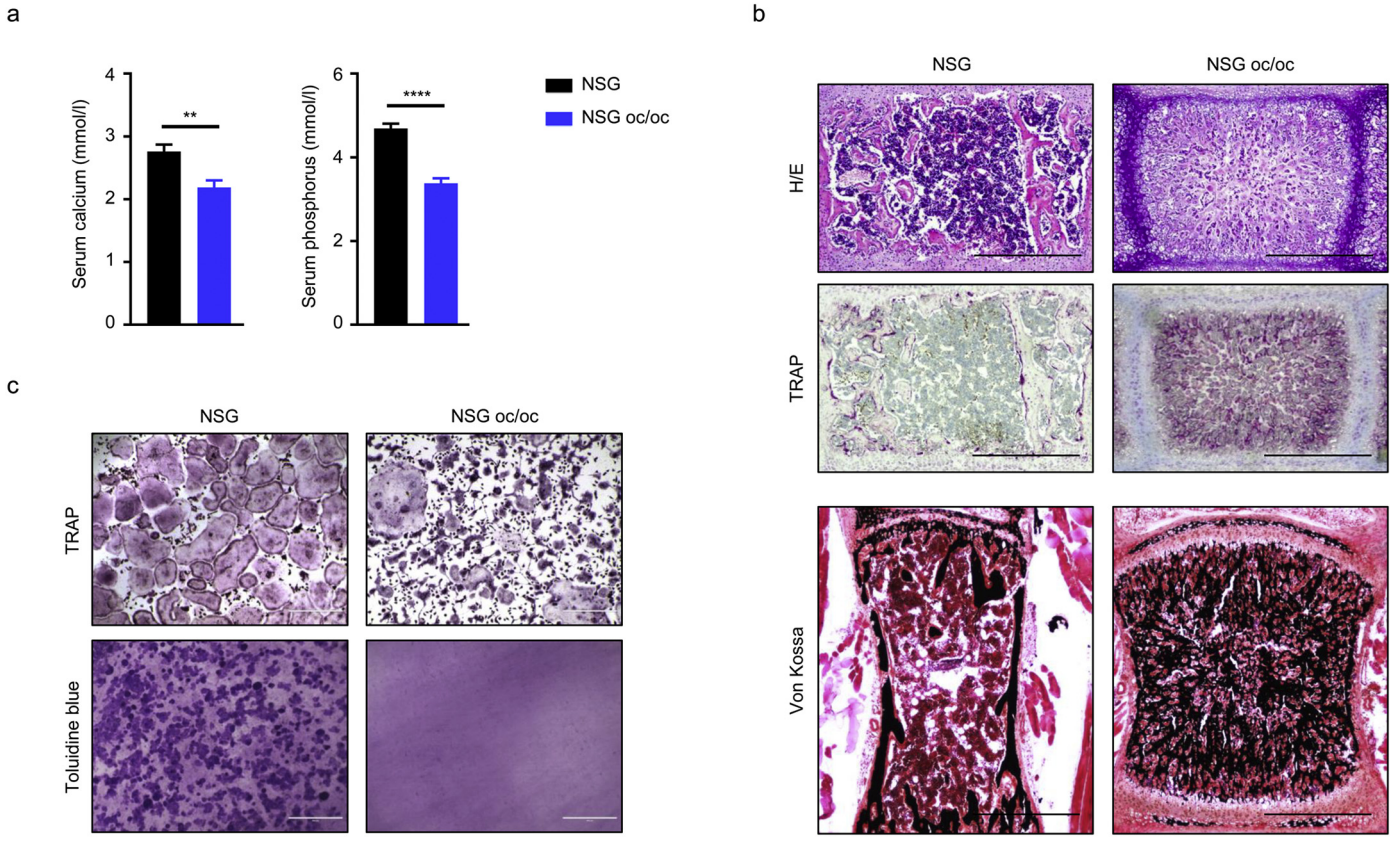

Fig. 3. NSG oc/oc mice present osteoclast-rich osteopetrosis. a Calcium and phosphorus serum levels in NSG and NSG oc/oc mice ($n \geq 8$ per genotype). **$p < 0.01$, ****$p < 0.0001$. b Representative images of decalcified formalin-fixed paraffin-embedded vertebral sections of NSG and NSG oc/oc mice stained with H/E (upper panels) and TRAP (middle panels); undecalcified formalin-fixed resin-embedded vertebral sections stained with von Kossa/van Gieson staining (lower panels). Scale bar: 500 μm. c *In vitro* osteoclastogenesis from splenic precursors of NSG and NSG oc/oc mice: representative images of TRAP staining on plastic (upper panels) and of Toluidine blue staining of resorption pits on dentin discs (lower panels). Scale bars: 400 μm.

NSG oc/oc mice as compared to controls, demonstrating a typical osteopetrotic appearance (Fig. 3b). TRAP staining was increased in NSG oc/oc mice, indicating that they displayed an osteoclast-rich form of osteopetrosis. Finally, von Kossa staining on non-decalcified resin-embedded tissue sections demonstrated an abnormal pattern of mineralization typical of rickets (Fig. 3b); this peculiar feature was previously described in the oc/oc mouse model and ascribed to defective gastric acidification in the absence of *Tcirg1* gene expression in gastric parietal cells, and reduced dietary calcium absorption (Schinke et al., 2009). Overall, the findings in NSG oc/oc mice mirrored those described in the oc/oc model (Scimeca et al., 2000; Schinke et al., 2009; Marks Jr. et al., 1985).

Finally, we evaluated *in vitro* osteoclast formation and bone resorption from NSG oc/oc and NSG splenic precursors according to standard protocols. In both cases, osteoclasts formed, but those generated from NSG oc/oc mice were mostly smaller and irregularly shaped (Fig. 3c), as previously observed in oc/oc osteoclasts (Nakamura et al., 1997), in line with the involvement of the V-ATPase in vesicle trafficking, in addition to its essential proton-pumping activity (Sobacchi et al., 2013). When differentiated on dentin, NSG osteoclasts generated well-developed resorption pits, while no sign of resorption was found in the presence of NSG oc/oc differentiated cells, thus demonstrating a complete functional impairment (Fig. 3c).

In conclusion, the NSG oc/oc mouse model displayed immunodeficiency and severe recessive osteoclast-rich osteopetrosis.

3.3. Neonatal murine bone marrow transplantation corrects the pathology in NSG oc/oc mice

Osteopetrosis in the oc/oc mouse derives from an osteoclast cell-autonomous defect, and in fact can be corrected by WT bone marrow transplantation (BMT) (Frattini et al., 2005; Johansson et al., 2006; Askmyr et al., 2009b; Flores et al., 2010). Therefore, we verified whether the same occurred in our NSG oc/oc mouse. In detail, NSG oc/oc and NSG neonates (P2-P4, $n = 6$ per group) were transplanted with BM cells from adult C57BL/6J WT mice after receiving a radiation dose of 100 cGy, and were sacrificed 3 or 12 weeks after transplant. In particular, the first time-point (*i.e.* 3 weeks post-BMT) allowed comparing the bone and spleen phenotype with that of untreated NSG oc/oc mice, which did not survive further, as mentioned above.

As early as 3 weeks after-BMT, μCT analysis of long bones showed complete normalization of the skeletal phenotype in transplanted NSG oc/oc mice (Fig. 4a). Of note, most of the measurements (*i.e.* bone volume over total volume ratio, BV/TV; bone surface over total volume ratio, BS/TV; trabecular number, Tb.N, and trabecular spacing, Tb.Sp) in transplanted NSG oc/oc mice overlapped those of untreated NSG and transplanted NSG mice. On the other hand, trabecular thickness (Tb.Th) did not differ among the different genotype and treatment groups (Fig. 4a). In parallel, axial bone histology showed substantial improvement of the bone defect in transplanted NSG oc/oc mice, with clear enlargement of the BM cavity and increase in BM cellularity (Fig. 4b). Accordingly, serological analysis showed no difference in calcium and phosphate levels in transplanted NSG oc/oc as compared to transplanted NSG mice (Fig. 4c), and normalization of these parameters in the former group as compared to untreated NSG oc/oc mice (see

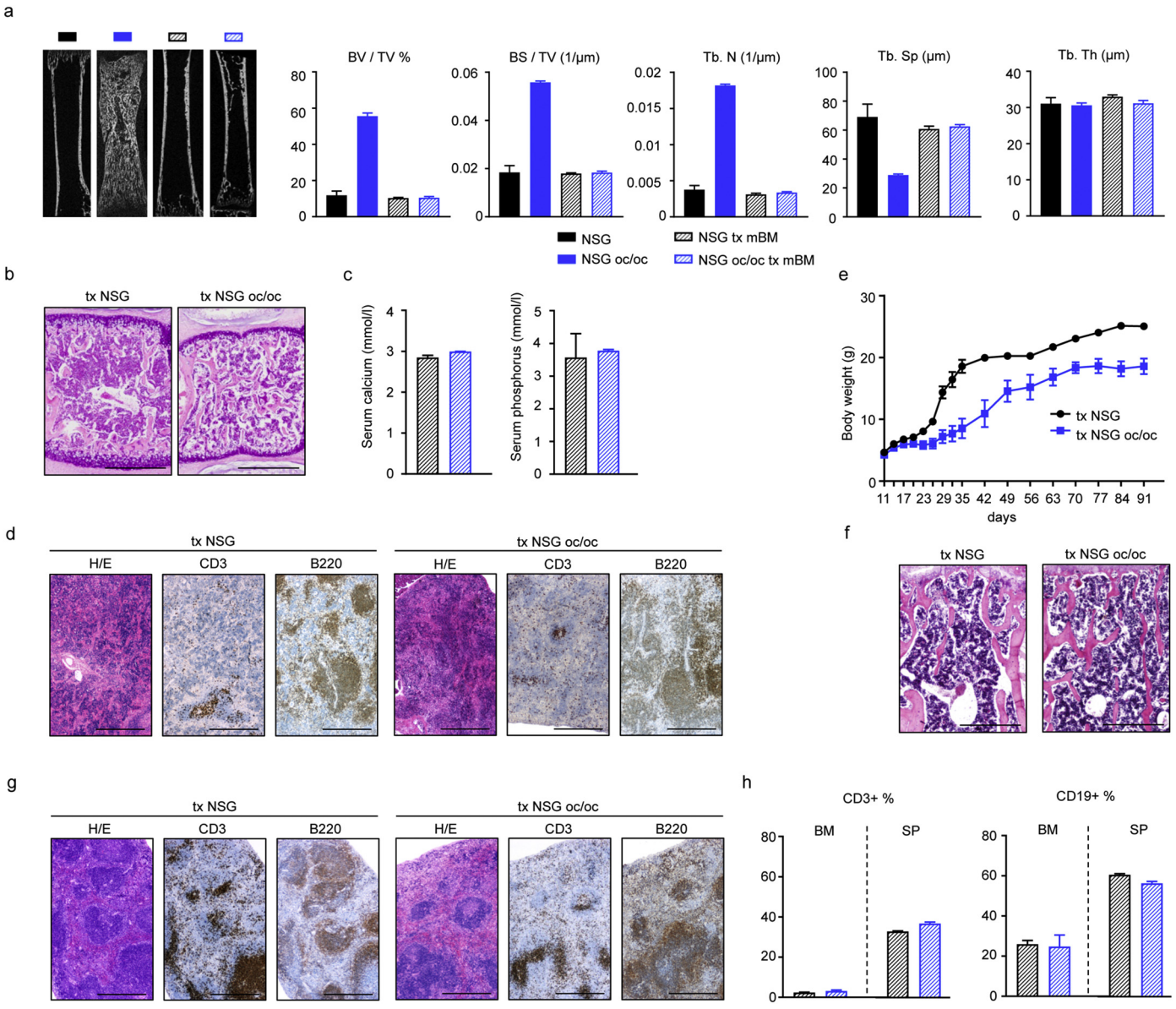

Fig. 4. Neonatal murine bone marrow transplantation corrects the pathology in NSG oc/oc mice. a MicroCT analysis of the femur of untreated NSG and NSG oc/oc mice, and murine BM-transplanted NSG and NSG oc/oc mice (n = 3 in all groups but transplanted NSG, where n = 2). b Representative images of decalcified formalin-fixed paraffin-embedded vertebral sections of transplanted (tx) NSG and NSG oc/oc mice 3 weeks after transplantation, stained with H/E. Scale bar: 500 μm. c Calcium and phosphorus serum levels in NSG and NSG oc/oc mice 3 weeks after transplantation (n = 2 per genotype; bars indicate the range). d Representative images of spleen of tx NSG and tx NSG oc/oc mice 3 weeks after transplantation, stained with H/E, anti-mouse CD3 or anti-mouse B220 antibody. Scale bar: 500 μm. e Growth curve of NSG and NSG oc/oc mice after transplantation, during the 3-month follow-up. f Representative images of decalcified formalin-fixed paraffin-embedded vertebral sections of transplanted (tx) NSG and NSG oc/oc mice 3 months after transplantation, stained with H/E. Scale bar: 500 μm. g Representative images of spleen of tx NSG and tx NSG oc/oc mice 3 months after transplantation, stained with H/E, anti-mouse CD3 or anti-mouse B220 antibody. Scale bar: 500 μm. h Histograms from FACS analysis of bone marrow (BM) and spleen (SP) cell suspensions from NSG and NSG oc/oc mice 3 months after transplantation (n = 3 per genotype).

Fig. 3a). Finally, H/E staining of the spleen demonstrated an initial attempt to restore red and white pulp separation, and IHC staining with specific antibodies documented the presence of partially compartmentalized T and B cells, both in NSG oc/oc and in NSG mice (Fig. 4d).

Mice that were kept under observation for 3 months after transplantation, gained weight over time, despite remaining smaller than control littermates (Fig. 4e) and in good health; of note, none of the transplanted NSG oc/oc mice showed the “circling behavior”. At this time point, histological analysis showed no difference between transplanted NSG and NSG oc/oc mice neither in the bone (Fig. 4f) nor in the spleen structure (Fig. 4g), which acquired a canonical pattern of tissue organization and cell distribution. Accordingly, cytofluorimetric analysis confirmed similar proportion of B and T cells in BM and spleen cell suspensions, in NSG and NSG oc/oc transplanted mice (Fig. 4h).

Overall, these data demonstrated that all the cell-autonomous defects (and specifically, osteoclast resorptive function) of the new mouse model could be rescued by BM transplantation, as previously observed for the oc/oc mouse (Frattini et al., 2005; Johansson et al., 2006; Askmyr et al., 2009b; Flores et al., 2010), highlighting the potential usefulness of our model to test novel cell therapy approaches for curing osteopetrosis, including preclinical studies with transduced murine progenitors.

3.4. NSG oc/oc mice are able to host human cells in their bone

NSG mice are widely used as models for xenotransplants, based on the capacity to support engraftment and development of human cells, conferred by their specific genetic background that prevents rejection. We speculated our new mouse model might serve as a xenograft model for the functional evaluation of gene-corrected human cells. To test this hypothesis, we performed human cell transplantation in neonate NSG oc/oc mice, owing to their severe phenotype impeding survival into adulthood. As donor cells, we exploited human $CD34^+$ cells from mobilized peripheral blood, as these are a relevant source for cell and gene therapy approaches to human osteopetrosis (Penna et al., 2019). In line with the above described experiments, here we irradiated NSG oc/oc mice and NSG controls (n = 7 and 2, respectively; age: P2-P4) sublethally with 100 cGy dose and infused $CD34^+$ cells in the temporal vein. Necropsy was performed on average 2 weeks later, after appearance of signs of suffering typical for the pathology (*i.e.* circling behavior and weight loss). Cytofluorimetric analysis of BM cell suspensions showed the presence of human $CD45^+$ cells in the NSG oc/oc (data not shown), indicating that, despite their severely compromised bone microenvironment, NSG oc/oc mice were able in principle to host human cells. However, the very low chimerism detected in the BM at this early time point (mean 1.65% ± 2.04 of human $CD45^+$ cells, median 0.6%; for the NSG controls, mean 2.46% ± 3.46, median 2.46% for the NSG oc/oc) was not sufficient for affecting the bone phenotype in such a short timeframe.

Thus, we decided to raise the radiation dose to 200 cGy in order to favor human cell engraftment by further depleting residual host cells occupying the BM or spleen stem cell niches. Nine NSG oc/oc and 6 NSG littermates were treated with this protocol; each mouse received on average 2×10^6 $CD34^+$ cells (range: 10^6–2.6×10^6 cells). Actually, also in this setting NSG oc/oc mice started displaying the pathology at about 2 weeks of age; sacrifice was performed 2–3 weeks after transplantation. FACS analysis of the BM revealed an increased chimerism as compared to the previous experimental setting (human $CD45^+$ cells in NSG oc/oc BM: mean 4.01% ± 1.31, median 3.46%; in NSG BM: mean 7.45% ± 3.1, median 5%), with some NSG oc/oc recipient mice showing up to 9–11% of human cells in their BM (Fig. 5a and b). Human cells were also present in the spleen (Fig. 5b). Importantly, human $CD14^+$ cells were detected in the BM of both NSG and NSG oc/oc mice (Fig. 5a and b), suggesting differentiation of human cells towards the myeloid lineage in the murine bone microenvironment, which is relevant in our disease model. Human $CD45^+$ cells could be detected also by IHC staining on bone (Fig. 5c; relevant controls for the IHC are shown in Supplementary Fig. 4). On the other hand, μCT analysis of bone demonstrated that the bone of transplanted NSG oc/oc mice remained osteopetrotic with no amelioration as compared to untreated NSG oc/oc mice (Fig. 5d), even though we cannot exclude that minor early modifications of the bone tissue might have occurred.

4. Discussion

Here we described the generation of a new mouse model of autosomal recessive osteopetrosis, which we named NSG oc/oc. This model carried the same genetic mutation as the well-known oc/oc mouse, since it was generated through a specific breeding strategy, and faithfully reproduced the key pathologic features of the parental strain. In addition, the NSG oc/oc mice displayed a complete lack of T, B and NK cells, which was the distinctive characteristic of the NSG strain.

To the best of our knowledge, there are no reports in literature of the very same approach (*i.e.* backcross of a disease-causing mutation into the NSG background for human hematopoietic stem cell transfer) carried out in the context of other disease models. For the sake of completeness, here we mention Brehm and colleagues, which generated

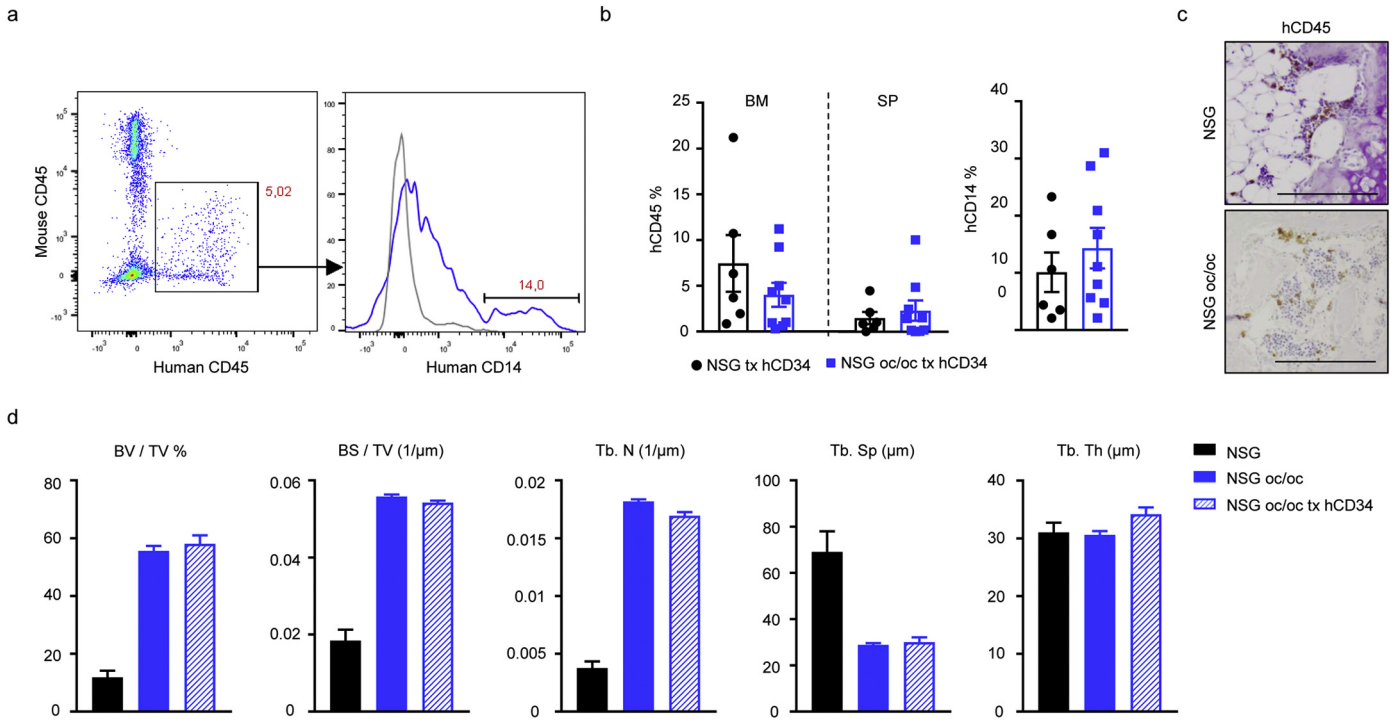

Fig. 5. Analysis of mice transplanted with human $CD34^+$ cells. a FACS analysis of the BM of a representative NSG oc/oc mouse 2 weeks after transplantation. Human $CD45^+$ leukocytes derived from transplanted $CD34^+$ cells were gated (left pseudocolor plot) and analyzed for the expression of the human CD14 monocyte marker (histogram on the right, blue line; gray line represents the Fluorescent-Minus-One control). b Scatter plots showing (left) the percentage of human $CD45^+$ leukocytes within the BM and the spleen of NSG and NSG oc/oc mice, and (right) the percentage of human $CD14^+$ cells within the BM. c Representative immunohistochemical staining of vertebral bone of transplanted mice two weeks after transplantation, showing the presence of human $CD45^+$ cells. Scale bar: 200 μm. d MicroCT analysis of the femur of NSG and NSG oc/oc mice (n = 3 per group) and NSG oc/oc mice transplanted with human cells (n = 5).

the spontaneously diabetic NRG-Akita mouse model by backcrossing the $Ins2^{Akita}$ mutation into the NOD-$Rag1^{null}$ $IL2r\gamma^{null}$ background (Brehm et al., 2010). However, owing to the rapid disease course and short life-span of mice homozygous for the $Ins2^{Akita}$ mutation, the authors performed all studies in mice heterozygous for the $Ins2^{Akita}$ allele.

The original purpose of our work was to provide the scientific community with an osteopetrotic mouse that might be used as a xenotransplant model to test *in vivo* the functional rescue of gene-edited patient-derived cells. In fact, since several years, studies are ongoing to develop a gene therapy approach to human osteopetrosis, with particular respect to the TCIRG1-deficient form that is the most common one (Johansson et al., 2007; Moscatelli et al., 2013; Thudium et al., 2016; Moscatelli et al., 2018); moreover, in recent years other tools for gene editing and cell therapy have been implemented (Maeder and Gersbach, 2016; Doss and Sachinidis, 2019). On the other hand, at a preclinical level demonstration of a functional rescue has been limited to *in vitro* assays (Moscatelli et al., 2013; Thudium et al., 2016; Moscatelli et al., 2018), while *in vivo* studies could demonstrate only the capacity of human corrected cells to engraft and differentiate in the host, not their resorbing capacity. Therefore, we intended to provide a missing tool in preclinical research.

Since the rapid and fatal progression of the disease impeded survival of transplanted NSG oc/oc mice, correction of the skeletal pathology could not be tested in the framework of the present work. Indeed, the major obstacle was represented by the severity of the disease: all NSG oc/oc mice generated in the framework of this study became very sick and had a rapid progression of their pathology, similarly to what observed in oc/oc mice (Scimeca et al., 2000). In this respect, the *Tcirg1*^{oc} mutation was invariably associated with a severe phenotype in the two different genetic backgrounds. Interestingly, in a previous work, oc/oc mice on a mixed (B6xC3x129) background were generated and, while the vast majority died at a mean age of 25 days, some of them survived up to 90 days (Blin-Wakkach et al., 2006). It is possible that, if our mouse model had had an extended life span, this could have been more compatible with the timing of human cell differentiation, which notoriously takes more time than murine cell differentiation (Abkowitz et al., 2000), and thus it could have possibly allowed achieving a benefit to the mouse from the transplanted human cells. However, by anticipating the xenotransplantation to the prenatal period, it could be possible to give transplanted cells more time to differentiate into functional osteoclasts, or at least into myeloid mature cells able to fuse with resident osteoclasts thereby rescuing their functional defect (Wakkach et al., 2008; Jacome-Galarza et al., 2019). In this regard, by performing *in utero* HSCT, we were able to rescue the osteopetrotic phenotype of oc/oc mice (Frattini et al., 2005; Tondelli et al., 2009); on the other hand, this kind of approach with human cells would be technically more challenging than with murine cells, requiring some refinement of the published protocol.

The transplant conditions we used, specifically the conditioning regimen, might raise some concern. Actually, despite being completely immunodeficient, NSG mice usually undergo myeloablative protocols prior to human cell transplantation, both when treated at the adult age and at the neonatal stage (Ishikawa et al., 2007; Cuddihy et al., 2012; Ko et al., 2017; Pang et al., 2019), and the radiation doses we used were in those ranges. In addition, the osteopetrotic bone is known to be a poorly permissive environment for cell engraftment, due to the lack of a proper niche, therefore a stronger host cell depletion is likely required to allow donor cell engraftment (Mansour et al., 2012). Accordingly, osteopetrotic patients are usually subjected to strong pretransplant conditioning, and only recent papers reported encouraging results in terms of outcome using reduced intensity conditioning (Bahr et al., 2016; Tolar et al., 2006; Shadur et al., 2018).

Last, osteoclast differentiation is known to crucially depend on the presence of RANKL and M-CSF. Indeed, mouse RANKL is known to be effective both on mouse and on human progenitors, at variance with mouse M-CSF which has been reported to be species specific (Gow et al., 2012). Therefore, it could be hypothesized that, if NSG oc/oc mice had survived longer, lack of human M-CSF might have anyway impeded human osteoclast formation in the murine bone. We considered this concern and conducted a pilot experiment in which together with xenotransplantation mice received repeated doses of human M-CSF; no improvement was observed in this experiment (data not shown), so this approach was not further pursued. Of note, other authors evaluated the possibility to induce ectopic expression of human M-CSF in $CD34^+$ cells, but this strategy blunted osteoclastogenesis, at least *in vitro* (Montano Almendras et al., 2017).

Humanized mice expressing human M-CSF are reported in the literature (Rathinam et al., 2011) and we might have considered the possibility to use that strain instead of NSG to generate our xenograft osteopetrotic mouse model. We did not undertake this strategy, so we do not know whether in that case the short lifespan of the model and severity of the disease might have still constituted an insuperable hurdle.

5. Conclusion

In summary, this work describes the generation and characterization of the NSG oc/oc mouse model of osteoclast-rich cell-autonomous Autosomal Recessive Osteopetrosis together with immunodeficiency. We show human cell chimerism in the bone marrow of NSG oc/oc mice transplanted with human $CD34^+$ cells. Exploitation of this new mouse model in the context of xenotransplants will likely require more attempts to set up experimental conditions, starting from our results, including for example infusion of human cytokines to foster differentiation, or further crossing with another genetic background. This notwithstanding, efforts would be likely worth the case, based on the importance of testing the functionality of human corrected cells in a relevant, live organism.

Supplementary data to this article can be found online at https://doi.org/10.1016/j.bonr.2020.100242.

Abbreviations

ARO	Autosomal Recessive Osteopetrosis
BM	Bone Marrow
BMT	Bone Marrow Transplantation
BS/TV	Bone Surface/Total Volume
BV/TV	Bone Volume/Total Volume
cGy	centiGray
Cs	Caesium
DAB	3-3'-Diaminobenzidine
EDTA	ethylenediaminetetraacetic acid
FBS	Fetal Bovine Serum
GFP	Green Fluorescent Protein
H/E	Hematoxylin/Eosin
HLA	Human Leukocyte Antigen
HSCT	Hematopoietic Stem Cell Transplantation
IHC	immunohistochemical
M-CSF	Macrophage-Colony Stimulating Factor
μCT	Micro-computed tomography
NSG	NOD Scid Gamma common chain
PBS	Phosphate-buffered saline
PCR	Polymerase chain reaction
PFA	paraformaldehyde
P/S	penicillin/streptomycin
RANKL	Receptor Activator of Nf-kB Ligand
Tb.N	Trabecular Number
Tb.Sp	Trabecular Spacing
Tb.Th	Trabecular Thickness
TGFβ	Transforming Growth Factor β
TRAP	Tartrate Resistant Acid Phosphatase
WT	wild type

Acknowledgements

We thank Fondazione Damiano per l'Ematologia and Fondazione Nicola del Roscio for their support to SM and LC, respectively (both, fellowship's assignees). We thank Dr. Ambra Rizzo (Laboratory of Clinical Pathology and Medical Genetics, Fondazione IRCCS Istituto Neurologico Carlo Besta) for the technical assistance.

Authors' contributions

PV conceived the project. PV, AV and HCB provided financial support. CS and FF designed and supervised the experiments. EP, SM, LC, ILT, DS, SM, EF and MM performed the experiments and measurements. SLL and CCS collected the human samples. EM, HCB, CS and FF analyzed the data. CS and FF wrote the manuscript. All authors reviewed and approved the final manuscript.

Funding

This work was partially supported by the EC Seventh Framework Programme (FP7/2007-2013, SYBIL Project, n. 602300) to AV, by the Ministry of Health, Italy (Grant n. PE-2011-02347329) to PV, and by the Department of Veterans Affairs (USA) grant I01BX002490 and the National Institutes of Health (USA) grant AR065407 to HCB.

Ethics approval

The study was approved by the Institutional Animal Care and Use Committee of Humanitas Clinical and Research Center and by the Italian Ministry of Health, protocol n.473/2017-PR.

Consent for publication

Not applicable.

Availability of data and materials

The data that support the findings of this study are included in this article or available from the corresponding author upon request.

Declaration of competing interest

The authors declare that they have no known competing financial interests or personal relationships that could have appeared to influence the work reported in this paper.

References

Abkowitz, J.L., Golinelli, D., Harrison, D.E., Guttorp, P., 2000. In vivo kinetics of murine hemopoietic stem cells. Blood 96 (10), 3399–3405.
Askmyr, M., Flores, C., Fasth, A., Richter, J., 2009a. Prospects for gene therapy of osteopetrosis. Current Gene Therapy 9 (3), 150–159.
Askmyr, M., Holmberg, J., Flores, C., Ehinger, M., Hjalt, T., Richter, J., 2009b. Low-dose busulphan conditioning and neonatal stem cell transplantation preserves vision and restores hematopoiesis in severe murine osteopetrosis. Exp. Hematol. 37 (2), 302–308.
Bahr, T.L., Lund, T., Sando, N.M., Orchard, P.J., Miller, W.P., 2016. Haploidentical transplantation with post-transplant cyclophosphamide following reduced-intensity conditioning for osteopetrosis: outcomes in three children. Bone Marrow Transplant. 51 (11), 1546–1548.
Blin-Wakkach, C., Breuil, V., Quincey, D., Bagnis, C., Carle, G.F., 2006. Establishment and characterization of new osteoclast progenitor cell lines derived from osteopetrotic and wild type mice. Bone 39 (1), 53–60.
Brehm, M.A., Bortell, R., Diiorio, P., Leif, J., Laning, J., Cuthbert, A., et al., 2010. Human immune system development and rejection of human islet allografts in spontaneously diabetic NOD-Rag1null IL2rgammanull Ins2Akita mice. Diabetes 59 (9), 2265–2270.
Castagna, L., Carlo-Stella, C., Mazza, R., Santoro, A., 2015. Current role of autologous and allogeneic stem cell transplantation for relapsed and refractory hodgkin lymphoma. Mediterranean Journal of Hematology and Infectious Diseases 7 (1), e2015015.
Crisafulli, L., Muggeo, S., Uva, P., Wang, Y., Iwasaki, M., Locatelli, S., et al., 2019. MicroRNA-127-3p controls murine hematopoietic stem cell maintenance by limiting differentiation. Haematologica 104 (9), 1744–1755.
Cuddihy, A.R., Suterwala, B.T., Ge, S., Kohn, L.A., Jang, J., Andrade, J., et al., 2012. Rapid thymic reconstitution following bone marrow transplantation in neonatal mice is VEGF-dependent. Biology of Blood and Marrow Transplantation: Journal of the American Society for Blood and Marrow Transplantation 18 (5), 683–689.
DiSanto, J.P., Muller, W., Guy-Grand, D., Fischer, A., Rajewsky, K., 1995. Lymphoid development in mice with a targeted deletion of the interleukin 2 receptor gamma chain. Proc. Natl. Acad. Sci. U. S. A. 92 (2), 377–381.
Doss, M.X., Sachinidis, A., 2019. Current challenges of iPSC-based disease modeling and therapeutic implications. Cells 8 (5).
Flores, C., de Vries, T.J., Moscatelli, I., Askmyr, M., Schoenmaker, T., Langenbach, G.E., et al., 2010. Nonablative neonatal bone marrow transplantation rapidly reverses severe murine osteopetrosis despite low-level engraftment and lack of selective expansion of the osteoclastic lineage. Journal of Bone and Mineral Research: The Official Journal of the American Society for Bone and Mineral Research 25 (9), 2069–2077.
Frattini, A., Orchard, P.J., Sobacchi, C., Giliani, S., Abinun, M., Mattsson, J.P., et al., 2000. Defects in TCIRG1 subunit of the vacuolar proton pump are responsible for a subset of human autosomal recessive osteopetrosis. Nat. Genet. 25 (3), 343–346.
Frattini, A., Blair, H.C., Sacco, M.G., Cerisoli, F., Faggioli, F., Cato, E.M., et al., 2005. Rescue of ATPa3-deficient murine malignant osteopetrosis by hematopoietic stem cell transplantation in utero. Proc. Natl. Acad. Sci. U. S. A. 102 (41), 14629–14634.
Fujiwara, S., 2018. Humanized mice: a brief overview on their diverse applications in biomedical research. J. Cell. Physiol. 233 (4), 2889–2901.
Gow, D.J., Garceau, V., Kapetanovic, R., Sester, D.P., Fici, G.J., Shelly, J.A., et al., 2012. Cloning and expression of porcine Colony Stimulating Factor-1 (CSF-1) and Colony Stimulating Factor-1 Receptor (CSF-1R) and analysis of the species specificity of stimulation by CSF-1 and Interleukin 34. Cytokine 60 (3), 793–805.
Ishikawa, F., Yoshida, S., Saito, Y., Hijikata, A., Kitamura, H., Tanaka, S., et al., 2007. Chemotherapy-resistant human AML stem cells home to and engraft within the bone-marrow endosteal region. Nat. Biotechnol. 25 (11), 1315–1321.
Jacome-Galarza, C.E., Percin, G.I., Muller, J.T., Mass, E., Lazarov, T., Eitler, J., et al., 2019. Developmental origin, functional maintenance and genetic rescue of osteoclasts. Nature 568 (7753), 541–545.
Johansson, M., Jansson, L., Ehinger, M., Fasth, A., Karlsson, S., Richter, J., 2006. Neonatal hematopoietic stem cell transplantation cures oc/oc mice from osteopetrosis. Exp. Hematol. 34 (2), 242–249.
Johansson, M.K., de Vries, T.J., Schoenmaker, T., Ehinger, M., Brun, A.C., Fasth, A., et al., 2007. Hematopoietic stem cell-targeted neonatal gene therapy reverses lethally progressive osteopetrosis in oc/oc mice. Blood 109 (12), 5178–5185.
Ko, Y., Jeong, Y.H., Lee, J.A., 2017. Transplantation of human umbilical cord blood CD34(+) cells into the liver of newborn NOD/SCID/IL-2Rgamma null (NSG) mice after busulfan conditioning. Blood Research 52 (4), 316–319.
Lo Iacono, N., Blair, H.C., Poliani, P.L., Marrella, V., Ficara, F., Cassani, B., et al., 2012. Osteopetrosis rescue upon RANKL administration to Rankl(−/−) mice: a new therapy for human RANKL-dependent ARO. Journal of Bone and Mineral Research: The Official Journal of the American Society for Bone and Mineral Research 27 (12), 2501–2510.
Maeder, M.L., Gersbach, C.A., 2016. Genome-editing technologies for gene and cell therapy. Molecular Therapy: The Journal of the American Society of Gene Therapy 24 (3), 430–446.
Mansour, A., Abou-Ezzi, G., Sitnicka, E., Jacobsen, S.E., Wakkach, A., Blin-Wakkach, C., 2012. Osteoclasts promote the formation of hematopoietic stem cell niches in the bone marrow. J. Exp. Med. 209 (3), 537–549.
Manz, M.G., Di Santo, J.P., 2009. Renaissance for mouse models of human hematopoiesis and immunobiology. Nat. Immunol. 10 (10), 1039–1042.
Marks Jr., S.C., Seifert, M.F., Lane, P.W., 1985. Osteosclerosis, a recessive skeletal mutation on chromosome 19 in the mouse. The Journal of Heredity 76 (3), 171–176.
Menale, C., Campodoni, E., Palagano, E., Mantero, S., Erreni, M., Inforzato, A., et al., 2019. MSC-seeded biomimetic scaffolds as a factory of soluble RANKL in Rankl-deficient osteopetrosis. Stem Cells Transl. Med. 8 (1), 22–34.
Montano Almendras, C.P., Thudium, C.S., Lofvall, H., Moscatelli, I., Schambach, A., Henriksen, K., et al., 2017. Forced expression of human macrophage colony-stimulating factor in CD34(+) cells promotes monocyte differentiation in vitro and in vivo but blunts osteoclastogenesis in vitro. Eur. J. Haematol. 98 (5), 517–526.
Moscatelli, I., Thudium, C.S., Flores, C., Schulz, A., Askmyr, M., Gudmann, N.S., et al., 2013. Lentiviral gene transfer of TCIRG1 into peripheral blood CD34(+) cells restores osteoclast function in infantile malignant osteopetrosis. Bone 57 (1), 1–9.
Moscatelli, I., Lofvall, H., Schneider Thudium, C., Rothe, M., Montano, C., Kertesz, Z., et al., 2018. Targeting NSG mice engrafting cells with a clinically applicable lentiviral vector corrects osteoclasts in infantile malignant osteopetrosis. Hum. Gene Ther. 29 (8), 938–949.
Nakamura, I., Takahashi, N., Udagawa, N., Moriyama, Y., Kurokawa, T., Jimi, E., et al., 1997. Lack of vacuolar proton ATPase association with the cytoskeleton in osteoclasts of osteosclerotic (oc/oc) mice. FEBS Lett. 401 (2–3), 207–212.
Neri, T., Muggeo, S., Paulis, M., Caldana, M.E., Crisafulli, L., Strina, D., et al., 2015. Targeted gene correction in osteopetrotic-induced pluripotent stem cells for the generation of functional osteoclasts. Stem Cell Reports 5 (4), 558–568.
Neven, B., Diana, J.S., Castelle, M., Magnani, A., Rosain, J., Touzot, F., et al., 2019. Haploidentical HSCT with post-transplant CY for primary immunodeficiencies and inherited disorders in children. Biology of Blood and Marrow Transplantation: Journal of the American Society for Blood and Marrow Transplantation 25 (7), 1363–1373.
Palagano, E., Blair, H.C., Pangrazio, A., Tourkova, I., Strina, D., Angius, A., et al., 2015. Buried in the middle but guilty: intronic mutations in the TCIRG1 gene cause human autosomal recessive osteopetrosis. Journal of Bone and Mineral Research: The

Official Journal of the American Society for Bone and Mineral Research 30 (10), 1814–1821.
Palagano, E., Menale, C., Sobacchi, C., Villa, A., 2018. Genetics of osteopetrosis. Current Osteoporosis Reports 16 (1), 13–25.
Pang, W.W., Czechowicz, A., Logan, A.C., Bhardwaj, R., Poyser, J., Park, C.Y., et al., 2019. Anti-CD117 antibody depletes normal and myelodysplastic syndrome human hematopoietic stem cells in xenografted mice. Blood 133 (19), 2069–2078.
Penna, S., Capo, V., Palagano, E., Sobacchi, C., Villa, A., 2019. One disease, many genes: implications for the treatment of osteopetroses. Front. Endocrinol. 10, 85.
Pronk, C.J., Turkiewicz, D., Vult von Steyern, K., Ehinger, M., Dykes, J., Toporski, J., 2017. Transplantation of haploidentical TcRass-depleted hematopoietic cells allows for optimal timing and sustained correction of the metabolic defect in children with infantile osteopetrosis. Journal of Bone and Mineral Research: The Official Journal of the American Society for Bone and Mineral Research 32 (1), 82–85.
Rathinam, C., Poueymirou, W.T., Rojas, J., Murphy, A.J., Valenzuela, D.M., Yancopoulos, G.D., et al., 2011. Efficient differentiation and function of human macrophages in humanized CSF-1 mice. Blood 118 (11), 3119–3128.
Schinke, T., Schilling, A.F., Baranowsky, A., Seitz, S., Marshall, R.P., Linn, T., et al., 2009. Impaired gastric acidification negatively affects calcium homeostasis and bone mass. Nat. Med. 15 (6), 674–681.
Scimeca, J.C., Franchi, A., Trojani, C., Parrinello, H., Grosgeorge, J., Robert, C., et al., 2000. The gene encoding the mouse homologue of the human osteoclast-specific 116-kDa V-ATPase subunit bears a deletion in osteosclerotic (oc/oc) mutants. Bone 26 (3), 207–213.
Shadur, B., Zaidman, I., NaserEddin, A., Lokshin, E., Hussein, F., Oron, H.C., et al., 2018. Successful hematopoietic stem cell transplantation for osteopetrosis using reduced intensity conditioning. Pediatr. Blood Cancer 65 (6), e27010.
Shultz, L.D., Lyons, B.L., Burzenski, L.M., Gott, B., Chen, X., Chaleff, S., et al., 2005. Human lymphoid and myeloid cell development in NOD/LtSz-scid IL2R gamma null mice engrafted with mobilized human hemopoietic stem cells. J. Immunol. 174 (10), 6477–6489.
Sobacchi, C., Villa, A., Schulz, A., Kornak, U., 1993. In: Adam, M.P., Ardinger, H.H., Pagon, R.A., Wallace, S.E., Bean, L.J.H., Stephens, K. (Eds.), CLCN7-Related Osteopetrosis. GeneReviews((R)), Seattle (WA).
Sobacchi, C., Schulz, A., Coxon, F.P., Villa, A., Helfrich, M.H., 2013. Osteopetrosis: genetics, treatment and new insights into osteoclast function. Nat. Rev. Endocrinol. 9 (9), 522–536.
Sobacchi, C., Pangrazio, A., Lopez, A.G., Gomez, D.P., Caldana, M.E., Susani, L., et al., 2014. As little as needed: the extraordinary case of a mild recessive osteopetrosis owing to a novel splicing hypomorphic mutation in the TCIRG1 gene. Journal of Bone and Mineral Research: The Official Journal of the American Society for Bone and Mineral Research 29 (7), 1646–1650.
Stattin, E.L., Henning, P., Klar, J., McDermott, E., Stecksen-Blicks, C., Sandstrom, P.E., et al., 2017. SNX10 gene mutation leading to osteopetrosis with dysfunctional osteoclasts. Sci. Rep. 7 (1), 3012.
Stepensky, P., Grisariu, S., Avni, B., Zaidman, I., Shadur, B., Elpeleg, O., et al., 2019. Stem cell transplantation for osteopetrosis in patients beyond the age of 5 years. Blood Advances 3 (6), 862–868.
Takenaka, K., Prasolava, T.K., Wang, J.C., Mortin-Toth, S.M., Khalouei, S., Gan, O.I., et al., 2007. Polymorphism in Sirpa modulates engraftment of human hematopoietic stem cells. Nat. Immunol. 8 (12), 1313–1323.
Teti, A., Econs, M.J., 2017. Osteopetroses, emphasizing potential approaches to treatment. Bone 102, 50–59.
Thudium, C.S., Moscatelli, I., Lofvall, H., Kertesz, Z., Montano, C., Bjurstrom, C.F., et al., 2016. Regulation and function of lentiviral vector-mediated TCIRG1 expression in osteoclasts from patients with infantile malignant osteopetrosis: implications for gene therapy. Calcif. Tissue Int. 99 (6), 638–648.
Tolar, J., Bonfim, C., Grewal, S., Orchard, P., 2006. Engraftment and survival following hematopoietic stem cell transplantation for osteopetrosis using a reduced intensity conditioning regimen. Bone Marrow Transplant. 38 (12), 783–787.
Tondelli, B., Blair, H.C., Guerrini, M., Patrene, K.D., Cassani, B., Vezzoni, P., et al., 2009. Fetal liver cells transplanted in utero rescue the osteopetrotic phenotype in the oc/oc mouse. Am. J. Pathol. 174 (3), 727–735.
Wakkach, A., Mansour, A., Dacquin, R., Coste, E., Jurdic, P., Carle, G.F., et al., 2008. Bone marrow microenvironment controls the in vivo differentiation of murine dendritic cells into osteoclasts. Blood 112 (13), 5074–5083.